STUDIES OF ETG TRANSPORT ON NSTX PLASMAS WITH GYROKINETICS AND REDUCED TRANSPORT MODELS

C. F. CLAUSER[*], T. RAFIQ, E. SCHUSTER, C. WILSON
Lehigh University
Bethlehem PA, USA
[*]Present address: Massachusetts Institute of Technology, Cambridge MA, USA
Email: cclauser@psfc.mit.edu

W. GUTTENFELDER, J. PARISI
Princeton Plasma Physics Laboratory
Princeton NJ, USA

G. AVDEEVA
Oak Ridge Associated Universities
Oak Ridge TN, USA

Abstract

A series of NSTX and NSTX-U plasmas are analysed to investigate the anomalous electron thermal transport caused by electron temperature gradient (ETG) modes. The high-fidelity gyrokinetic code CGYRO is employed to carry out extensive linear and nonlinear ETG simulations. Linear gyrokinetic simulations are performed to determine ETG thresholds in different discharges, and they are compared with the simple scaling formula derived for conventional tokamaks. Results are also compared with reduced models to better understand their applicability in spherical tokamaks as well as in future reactor conditions. Nonlinear gyrokinetic simulations are conducted for selected cases to calculate electron thermal transport and compare the results with those of ETG modes in the Multi-Mode Model (MMM) and the Trapped-Gyro-Landau-Fluid (TGLF) reduced model codes.

1. INTRODUCTION

Experiments on NSTX have demonstrated that electron thermal transport is anomalous and dominates over ion thermal transport, which has been reported to usually be at neoclassical levels [1,2]. One of the modes that is responsible for electron thermal transport is the electron temperature gradient (ETG) mode [3]. To properly model anomalous transport in tokamaks and, in particular, the transport caused by ETG modes, gyrokinetics is commonly used and has also been proven to be accurate in spherical tokamaks [3]. However, it is expensive for fast or real-time profile reconstruction and, in some cases, for profile prediction. Therefore, reduced models need to capture ETG physics, namely thresholds and transport, in order to be used for predicting profiles in present and future devices like NSTX and NSTX-U. Hence, validating these models against gyrokinetic simulations is critical.
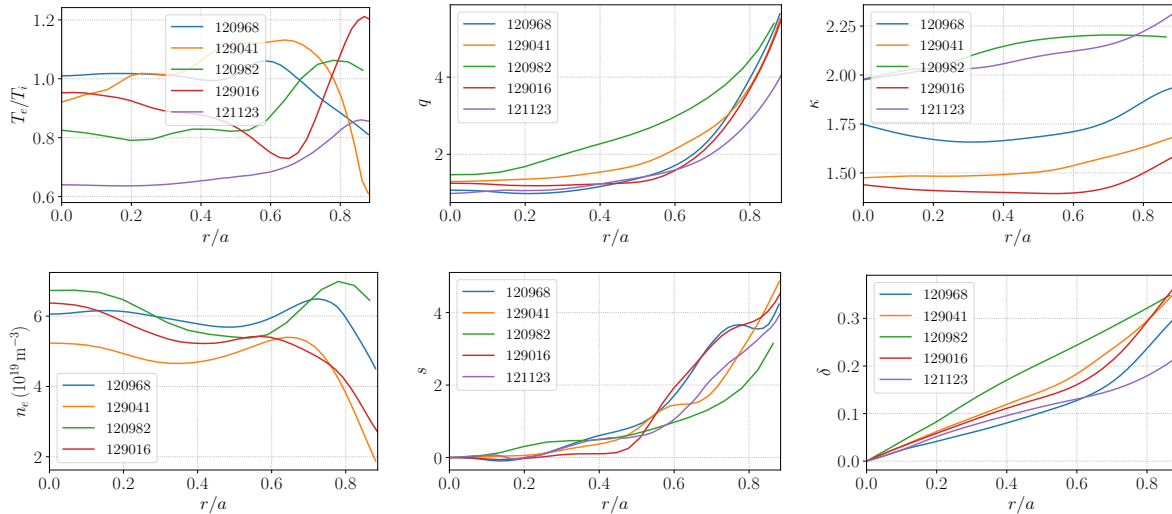
FIG. 1. NSTX profiles of the different shots analyzed with linear simulations. Figure shows ratio of electron to ion temperatures, T_e/T_i, safety factor, q, elongation, κ, electron density, n_e, magnetic shear, s, and triangularity, δ.

In this work, an extensive linear analysis of ETG modes was carried out in NSTX plasmas. Nonlinear simulations to study ETG transport were also performed for particular cases. All the simulations were conducted using the CGYRO code [4]. Figure 1 shows various profiles of the different analysed discharges in this work that can affect ETG stability.

TABLE 1.   SUMMARY OF RELEVANT EQUILIBRIUM PARAMETERS AT THE DIFFERENT RADIAL LOCATIONS OF THE ANALYSED SHOTS.

(a) NSTX #120968A02 at 560 ms

r/a	κ	δ	q	s	$\beta_{e,unit}$	T_e/T_i	a/L_{T_e}	a/L_{n_e}	$\alpha_{MHD,u}$	Z_{eff}	ν^{ei}	$\gamma_E(c_s/a)$
0.4	1.66	0.080	1.16	0.61	5.15	1.00	1.56	0.307	0.359	2.06	1.27	0.152
0.6	1.71	0.127	1.70	1.70	2.51	0.944	2.66	-0.774	0.412	2.87	3.91	0.174
0.7	1.76	0.166	2.47	3.16	1.39	1.02	3.11	-0.469	0.416	2.86	7.54	0.118
0.8	1.86	0.237	3.97	3.60	0.588	1.13	2.80	2.60	1.28	2.77	11.7	0.088

(b) NSTX #129016A03 at 460 ms

r/a	κ	δ	q	s	$\beta_{e,unit}$	T_e/T_i	a/L_{T_e}	a/L_{n_e}	$\alpha_{MHD,u}$	Z_{eff}	ν^{ei}	$\gamma_E(c_s/a)$
0.4	1.40	0.111	1.23	0.104	3.44	1.14	0.982	0.076	0.150	1.47	0.778	0.402
0.6	1.40	0.161	1.58	1.93	1.93	1.33	3.48	0.379	0.594	1.68	1.91	0.757
0.7	1.43	0.211	2.32	3.09	0.869	1.27	3.28	1.10	0.839	1.95	4.24	0.408
0.8	1.50	0.293	3.69	3.71	0.357	0.92	2.07	3.33	0.882	2.50	7.12	0.060

(c) NSTX #129041A10 at 490 ms

r/a	κ	δ	q	s	$\beta_{e,unit}$	T_e/T_i	a/L_{T_e}	a/L_{n_e}	$\alpha_{MHD,u}$	Z_{eff}	ν^{ei}	$\gamma_E(c_s/a)$
0.4	1.49	0.119	1.54	0.37	3.77	0.941	0.37	-0.299	0.129	3.23	0.71	0.144
0.6	1.54	0.184	2.13	1.45	2.65	0.888	1.44	-0.545	0.392	3.33	1.07	0.163
0.7	1.58	0.235	2.70	1.78	1.70	0.901	2.07	1.21	1.02	4.07	1.80	0.132
0.8	1.63	0.295	3.75	3.30	0.626	1.06	4.95	5.75	1.76	4.75	2.78	0.138

(d) NSTX #120982A09 at 620 ms

r/a	κ	δ	q	s	$\beta_{e,unit}$	T_e/T_i	a/L_{T_e}	a/L_{n_e}	$\alpha_{MHD,u}$	Z_{eff}	ν^{ei}	$\gamma_E(c_s/a)$
0.4	2.15	0.170	2.27	0.488	1.90	1.20	0.453	0.398	0.300	1.55	0.355	0.119
0.6	2.20	0.244	2.97	0.972	1.17	1.15	1.59	-0.931	0.543	1.78	0.578	0.297
0.7	2.20	0.282	3.55	1.36	0.933	0.983	2.19	-1.53	0.486	2.23	1.22	0.211
0.8	2.20	0.321	4.43	2.11	0.627	0.941	3.01	0.348	1.15	2.41	2.28	0.093

(e) NSTX-U #121123K55 at 14.5 s

r/a	κ	δ	q	s	$\beta_{e,unit}$	T_e/T_i	a/L_{T_e}	a/L_{n_e}	$\alpha_{MHD,u}$	Z_{eff}	ν^{ei}	$\gamma_E(c_s/a)$
0.4	2.06	0.096	1.23	0.5	3.68	1.53	0.454	0.75	0.325	2.0	0.178	0.048
0.6	2.12	0.131	1.59	1.05	1.88	1.46	2.04	1.22	0.695	2.0	0.219	0.129
0.7	2.15	0.149	2.03	2.17	1.09	1.36	3.04	-0.045	0.623	2.0	0.339	0.098
0.8	2.22	0.179	2.87	3.05	0.544	1.21	3.82	0.973	0.883	2.0	0.621	0.0183

NSTX shots 120968, 129041 and 120982 were already employed in ion scale analysis, and they were referred to as high, medium, and low collisionality discharges [5]. The NSTX-U projection #121123 was also studied in the same work and referred to an even lower collisionality regime, which is one of the main purposes of NSTX-U [6]. The shot #129016 was also explored in the past, when the first ETG gyrokinetic simulations in NSTX were presented [3]. As can be noted, profiles cover a wide range of conditions. A more complete set of parameters can be found in Table 1. For all the simulations, three kinetic species were included: electrons, deuterons (the main plasma ion species), and carbon as the main impurity.

2.   LINEAR GYROKINETIC ANALYSIS

As a first step and for each discharge, linear simulations were conducted over a wide range of wavenumbers to determine the modes present at the nominal experimental conditions. Figure 2(a-b) shows the real frequency and the growth rate for the shot 129016 at two radial locations, $r/a = 0.6$ and 0.7, as a function of the binormal wavenumber, $k_\theta \rho_s$. It can be seen that, at $r/a = 0.6$ the dominant mode is ETG with microteating modes (MTMs) being present with very low growth rates. At $r/a = 0.7$ different modes are present, including kinetic ballooning modes (KBMs), in addition to MTMs and ETG modes. In both cases, the $E \times B$ flow shear is larger and expected to suppress this ion scale instability (although MTMs can sometimes be unaffected by the flow shear rate). Figure 2(c-d) shows eigenfunctions of the perturbed electrostatic potential, $\delta\varphi$, and the perturbed parallel vector potential, $\delta A_\parallel$, for a mode with $k_\theta \rho_s = 20$ at $r/a = 0.6$. The eigenfunctions show twisting parity, which is a feature of an ETG mode.
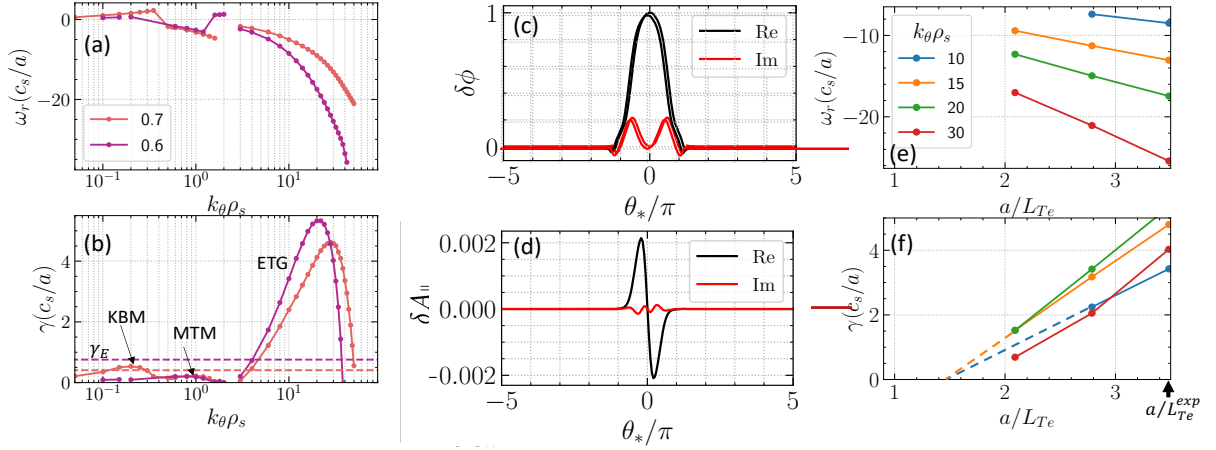
FIG. 2. Linear analysis of the 129016 discharge. (a) real frequency and (b) growth rate. Eigenfunctions for (c) the perturbed electrostatic potential and (d) the perturbed parallel vector potential. A scan over the electron temperature gradient is shown in (e) and (f) to determine the ETG growth rate threshold.

In order to determine ETG thresholds, scans over the electron temperature gradient scale length, $a/L_{T_e} = -(a/T_e)\ dT_e/dr$, were performed for a wide range of wavenumbers. Figure 2(e-f) shows an example of these scans for the shot 129016 at $r/a = 0.6$.

A similar procedure as the one described for Fig. 2 was conducted for all the different discharges, in which the critical gradient was determined for the radial region $r/a = 0.4 - 0.8$. A summary of the results is presented in Fig. 3, which shows the experimental temperature gradient profile as $\left(R/L_{T_e}\right)^{(exp)}$, along with the ETG critical gradient (or threshold) inferred from the linear gyrokinetic simulations, $\left(R/L_{T_e}\right)^{(GK)}_{ETG}$. Figure 3 also includes a simple scaling expression, $\left(R/L_{T_e}\right)^{(J)}_{ETG} = \max\{(1 + Z_{eff}T_e/T_i)(1.33 + 1.91\ s/q)(1 - 1.5\epsilon)(1 + 0.3\ r\ d\kappa/dr),\ 0.8\ R\ L_{n_e}\}$, derived for conventional tokamaks [7]. By comparing the inferred threshold from GK simulations with the experimental value, it is clear that ETG modes are present in several cases while suppressed in others.
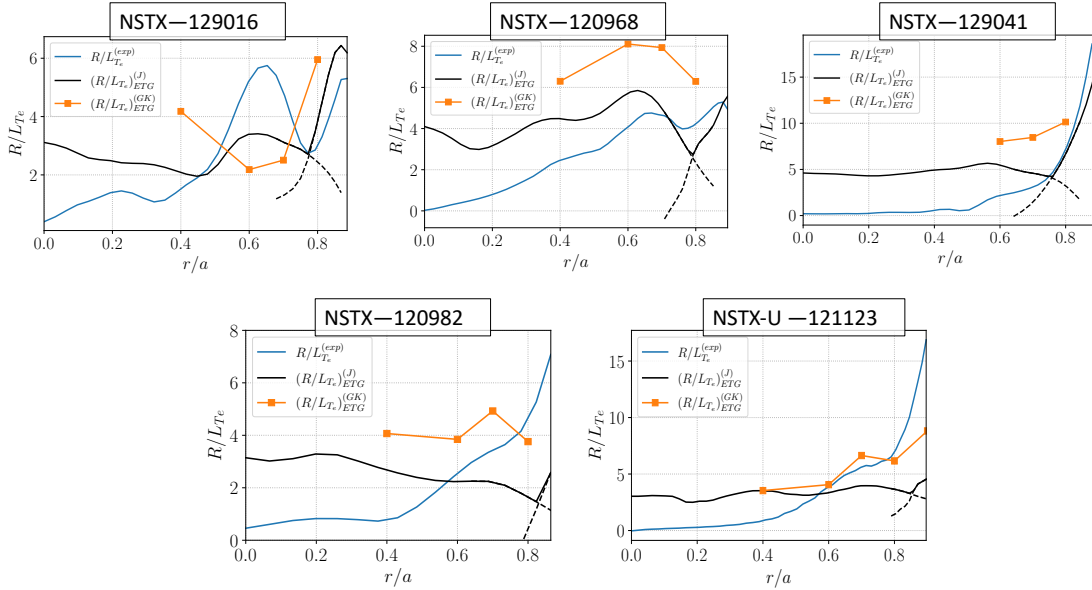
FIG. 3. ETG threshold profiles inferred from CGYRO linear simulations, $\left(R/L_{T_e}\right)^{(GK)}_{ETG}$, for four different NSTX discharges and one NSTX-U projection. The experimental nominal profile, $R/L_{T_e}^{(exp)}$, and an analytic expression derived for conventional tokamaks, $\left(R/L_{T_e}\right)^{(J)}_{ETG}$, are included for reference.

Another observation is that the $\left(R/L_{T_e}\right)^{(J)}_{ETG}$ expression is not in good agreement with $\left(R/L_{T_e}\right)^{(GK)}_{ETG}$ which exposes the limitation of this formula when applied to low aspect ratio spherical tokamaks. To put in evidence the complex physics that impact the scaling properties of ETG thresholds in this regime, scans over magnetic shear, s, elongation, κ, and safety factor, q, were conducted over the different discharges. Figure 4 shows the results for shots 129016 and 120982. It can be noted that very different behavior arises in both cases: ETG threshold increases with magnetic shear for shot 129016 as it does for standard tokamaks. However, the opposite trend occurs for shot 120982. When scaling over elongation, both cases show a threshold from which the ETG threshold starts to increase and become sensitive to the plasma elongation.
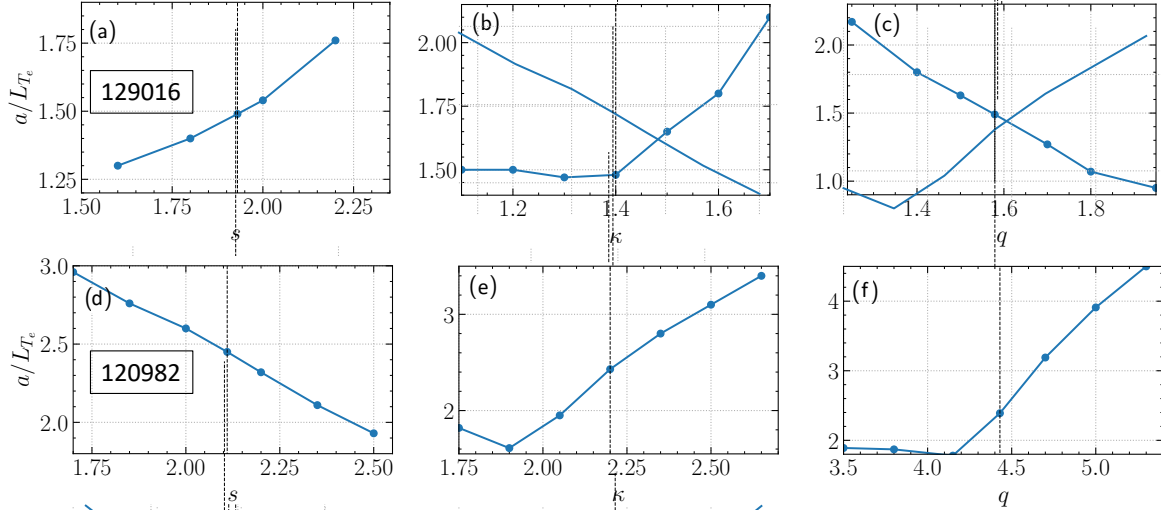
FIG. 4. ETG threshold inferred from linear CGYRO simulations for shot 129016 (upper panel) and shot 120982 (lower panel) as a function of magnetic shear, s, elongation, κ, and safety factor, q. The trend observed in the first case agrees with standard ETG thresholds while in the second case, the role of δB∥ seems to play an important role.

Finally, the scan over the safety factor also reveals opposite trends: the threshold decreases as the safety factor increases for shot 129016, similarly to conventional tokamaks, but it shows a threshold after which it increases for shot 120982. To better understand the different ETG threshold behaviour in shot 120982, an analysis is presented in Fig. 5, showing (a) real frequencies and (b) growth rates over a wide range of wavenumbers, and for different electron temperature gradients scaling factor ("1.0" means the experimental value of a/L_{T_e} = 3.01).
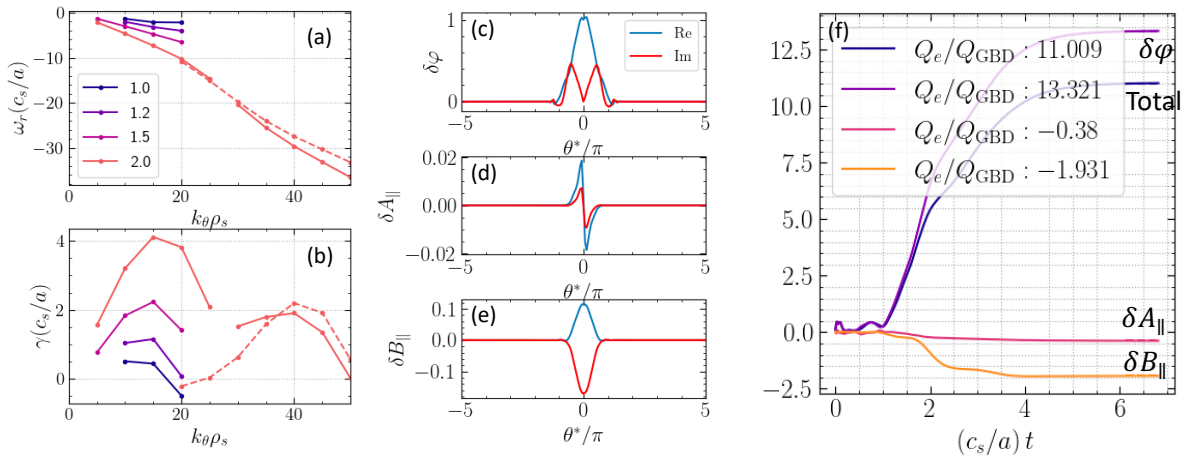
FIG 5. Analysis of the ETG threshold for the shot 120982 at r/a = 0.8. (a-b) shows real frequency and growth rates for different electron temperature gradient scaling factor (1.0 means the experimental condition). The dashed line show results when turning δB∥ off. (c-e) show the eigenfunction for the $k_\theta \rho_s$ = 10 mode, corresponding to a twisting parity mode. (f) shows the electron thermal (linear) flux with its different field contribution.

It can be seen that growth rates peaking at $k_\theta \rho_s \sim 10$ are very sensitive to the electron temperature gradient, in agreement with ETG modes. Another peak arises at $k_\theta \rho_s \sim 40$ after doubling the experimental nominal value. The dashed line shows the result when turning $\delta B_\parallel$ off. It is clear that the first peak vanishes when the parallel magnetic field perturbation is not included while the second peak is more resilient, as it is the usual case of ETG modes. However, Fig. 5(c-e) shows that the eigenfunction of the $k_\theta \rho_s \sim 10$ mode presents a ballooning or twisting parity. In addition, Fig. 5(f) shows that the electron thermal flux is mostly due to the electrostatic potential (although the parallel magnetic field contribution is important). Therefore, these modes peaking at $k_\theta \rho_s \sim 10$ are ETG modes, but they are rather sensitive to the compressional magnetic field, making them behave differently from standard ETG modes. A simple formula like the ones used for conventional tokamaks might not be enough to describe ETG critical gradients in these conditions. Scaling laws for ETG threshold in spherical tokamaks should consider additional effects that arise in high-β low aspect ratio tokamaks.

3. NON-LINEAR GYROKINETIC ANALYSIS

In this section, nonlinear gyrokinetic analysis is conducted to assess the thermal transport caused by ETG modes and to compare it with reduced models. In particular, the shot 129016 was analysed at r/a=0.6 and 0.7. As a first step, a convergence analysis was performed. CGYRO uses spectra and pseudospectral techniques in four of the five dimensions. To test convergence, radial (N_{rad}) and binormal (N_{tor}) grid resulotion were changed. Table 2 shows the different values chosen as well as other related quantities employed in the simulations.

TABLE 2.   CGYRO RESOLUTIONS TO TEST CONVERGENCE

Case	N_{rad}	N_{tor}	$\Delta k_x \rho_s$	$\Delta k_\theta \rho_s$	L_x / ρ_s	L_y / ρ_s
A	96	26	1.82	3	3.5	2.1
B	144	26	1.01	3	6.2	2.1
C	144	34	1.03	2.2	6.1	2.9

The remaining grid resolution values were: $n_\theta = 48$, $n_\xi = 16$, and $n_\varepsilon = 8$. Figure 6(a) shows the electron thermal flux evolution during the simulation, which clearly saturates for all cases, described in Table 2. The dashed line represents an average value that is shown for reference.
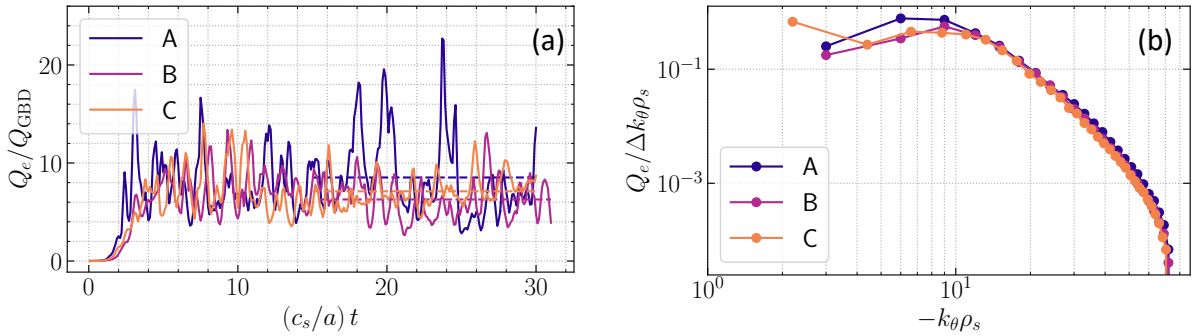
FIG. 6. (a) Total electron thermal flux evolution showing saturation for three different grid resolutions. (b) thermal flux spectra averaging over the time window indicated with the dashed lines in (a).

In addition, Fig. 6(b) shows the electron thermal flux spectra during the saturated phase. It is easy to see that the turbulent cascade is well covered, with a peak around $k_\theta \rho_s \sim 9 - 10$.

To assess the effect of the flow shear rate, and to account for uncertainties in the nominal value of the electron temperature gradients, nonlinear simulations were performed, varying both quantities. This is shown in Fig. 7, where thermal flux spectra are presented for different values of γ_E and a/L_{T_e}. The $E \times B$ flow shear rate has an impact on low-$k_\theta \rho_s$, as expected, while increasing the electron temperature gradient impacts the entire spectrum since a broader range of modes becomes unstable.
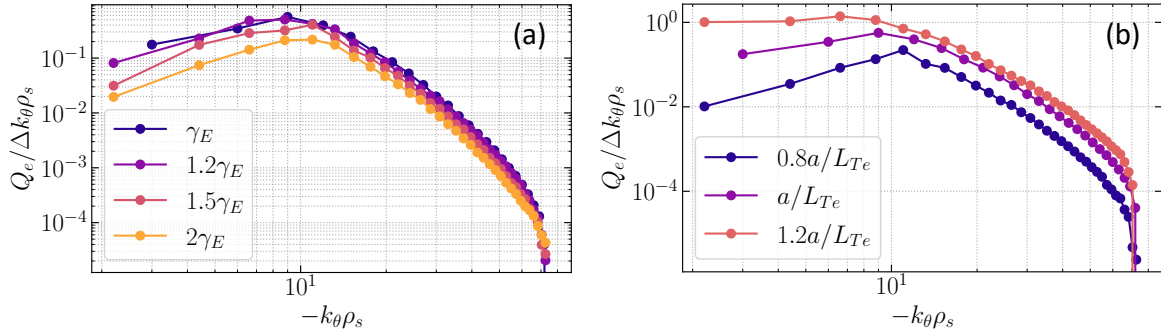
FIG. 7. ETG electron thermal flux spectra for (a) different $E \times B$ flow shearing rates, γ_E, and for (b) different values of the electron temperature gradient, a/L_{T_e}. Lower $k_\theta \rho_s$ modes are affected by γ_E, while a/L_{T_e} affects the entire spectra.

4. POWER FLOW AND COMPARISON WITH REDUCED MODELS

In this section, linear and nonlinear CGYRO results are compared with reduced models. Figure 8 shows real frequency and growth rate of the shot 129016 presented in Fig. 2 but compared with a reduced model developed for ETG modes, ETGM [8], as well as TGLF [9], which has been widely used in conventional tokamaks. Both reduced models find unstable ETG modes at this condition, in agreement with CGYRO. Real frequencies at $r/a = 0.6$ are well reproduced by both reduced models. TGLF also reproduces the real frequency at $r/a = 0.7$ in good agreement with CGYRO. However, some discrepancies occur in the growth rates. At $r/a = 0.6$ ETGM growth rate presents a similar behavior to CGYRO matching the maximum growth rate value, although the overall trend is shifted towards lower wavenumbers. TGLF also presents growth rates trends similar to CGYRO but they are systematically overpredicted. This overprediction of TGLF was already pointed out in other studies [10].
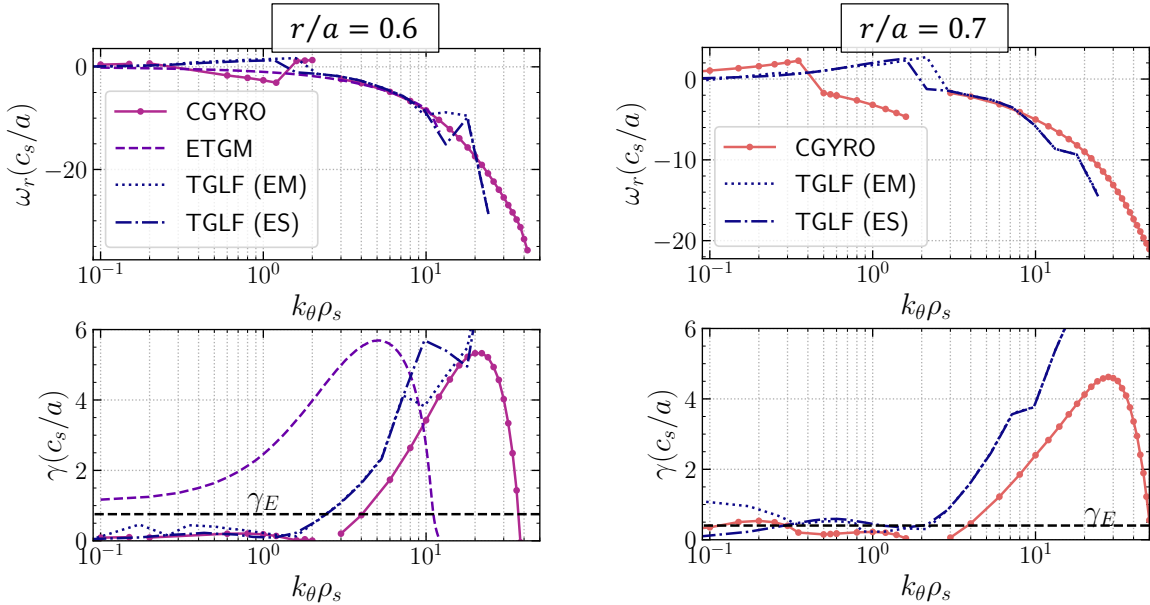
FIG. 8. Comparison of CGYRO linear simulations (real frequency and growth rates) with reduced models ETGM and TGLF for shot 129016 at two radial locations, $r/a = 0.6$ (left) and 0.7 (right).

Nonlinear simulations presented in the previous section allow the calculation of the total power flow. This is presented in Fig. 9, which shows the total power flow through the (a) $r/a = 0.6$ and (b) 0.7 flux surfaces for the shot 129016 as a function of the electron temperature gradient. The experimental result is marked with a black star, and a 20% error bar is assumed. From the linear analysis, it is reasonable to expect that, for r/a=0.6, all the transport is caused by ETGs, while at r/a=0.7, KBMs can play a role since they are near threshold.

CGYRO results are shown for three flow shear rates in both cases (at r/a=0.6, $\gamma_E = 0.757\, c_s/a$, and at r/a=0.7, $\gamma_E = 0.403\, c_s/a$). Simulations were also conducted over three values of the electron temperature gradient, to account for experimental uncertainties.
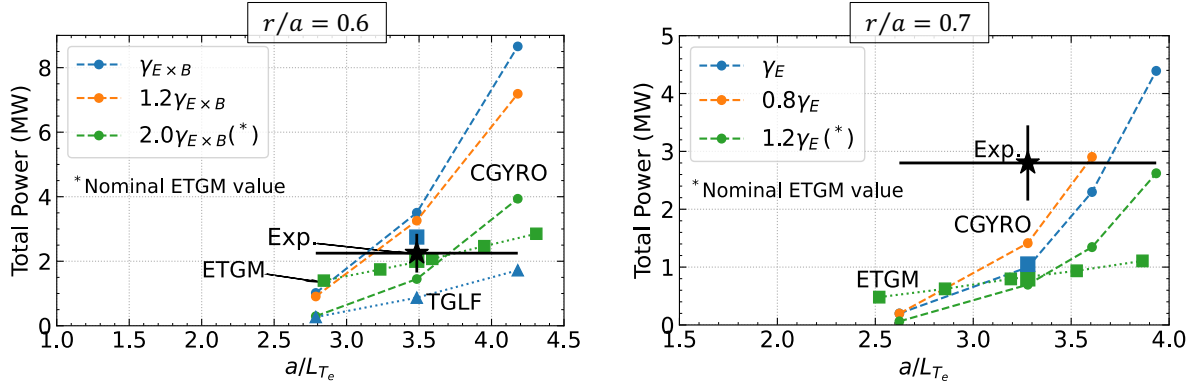
FIG. 9. Power flow through the flux surface $r/a = 0.6$ (left) and 0.7 (right) for shot 129016. Experimental value is indicated with a black star with a 20% generic error is assumed. CGYRO results are indicated with circles and colors refer to different values of flow shearing rates γ_E.

It can be observed that the comparison with NSTX experimental data is in good agreement within the uncertainties. The possible underprediction at r/a=0.7 against the experimental nominal value could rely on the fact that MTMs are just above threshold for that condition and can account for a significant transport, while the simulations only include the transport caused by ETG modes. In addition, Fig. 9 shows results from the reduced model ETGM [8], which are in excellent agreement with the experimental nominal value at r/a=0.6, and with the CGYRO simulations in both cases. This provides strong confidence for the use of ETGM for profile prediction in future NSTX-U discharges. The results of the reduced model TGLF [9] are also included at r/a=0.6 for comparison, which properly identify the presence of ETG modes, but underpredicts in this case the total power flow. It is important to note that the scaling of the power flow with the electron temperature gradient is different for CGYRO and both reduced models. Both ETGM and TGLF exhibit similar linear scaling behavior, in contrast to CGYRO, which displays a power-law-like trend. This discrepancy warrants further investigation and understanding.

5. CONCLUSIONS

Extensive linear gyrokinetic simulations were conducted on several NSTX discharges and on an NSTX-U projection to analyze the occurrence and thresholds of ETG modes. The discharges covered a wide range of parameter space. ETG threshold profiles were determined, finding that the modes are usually present in some discharges while suppressed in others at the experimental value. The ETG threshold in spherical tokamaks is shown to follow a more complex physics that cannot in principle be described by a simple analytic formula since different trends are observed in different cases. A comparison of gyrokinetic simulations with reduced models, critical for fast profile prediction, was also conducted. Both ETGM and TGLF models captured ETG physics, with transport levels comparable to those predicted by CGYRO. In particular, the ETGM model has shown power flow close to experimental values, as have the CGYRO results with nonlinear simulations. The scaling of the power flow with the electron temperature gradient shows some differences between CGYRO, which shows a power-like trend, and ETGM and TGLF reduced models, which show a more linear-like trend.

REFERENCES

[1] KAYE, S. M., BELL, R. E., GATES, D., et al., Phys. Rev. Lett. 98 (2007) 175002.

[2] KAYE, S., LEVINTON, F., STUTMAN, D., et al., Nucl. Fusion 47 (2007) 499.

[3] GUTTENFELDER, W., PETERSON, J., CANDY, J., et al., Nuclear Fusion 53 (2013) 093022.

[4]   CANDY, J., BELLI, E., and BRAVENEC, R., Journal of Computational Physics 324 (2016) 73.

[5]   CLAUSER, C. F., GUTTENFELDER, W., RAFIQ, T., et al., Physics of Plasmas 29 (2022) 102303.

[6]   GUTTENFELDER, W., BATTAGLIA, D., BELOVA, E., et al., Nucl. Fusion 62 (2022) 042023.

[7]   JENKO, F., DORLAND, W., and HAMMETT, G. W., Physics of Plasmas 8 (2001) 4096.

[8]   RAFIQ, T., WILSON, C., LUO, L., et al., Physics of Plasmas 29 (2022).

[9]   STAEBLER, G. M. and KINSEY, J. E., Physics of Plasmas 17 (2010) 122309.

[10] AVDEEVA, G., THOME, K., SMITH, S., et al., "Energy transport analysis of NSTX plasmas with the TGLF turbulent and NEO neoclassical transport models", Nuclear Fusion 2023 (submitted).